ACS OMEGA

http://pubs.acs.org/journal/acsodf

Article

Characterization of Cellulose−Chitosan-Based Materials from Different Lignocellulosic Residues Prepared by the Ethanosolv Process and Bleaching Treatment with Hydrogen Peroxide

Suchat Pongchaiphol, Thanchanok Preechakun, Marisa Raita,* Verawat Champreda, and Navadol Laosiripojana

Cite This: *ACS Omega* 2021, 6, 22791−22802

Read Online

ACCESS | Metrics & More | Article Recommendations

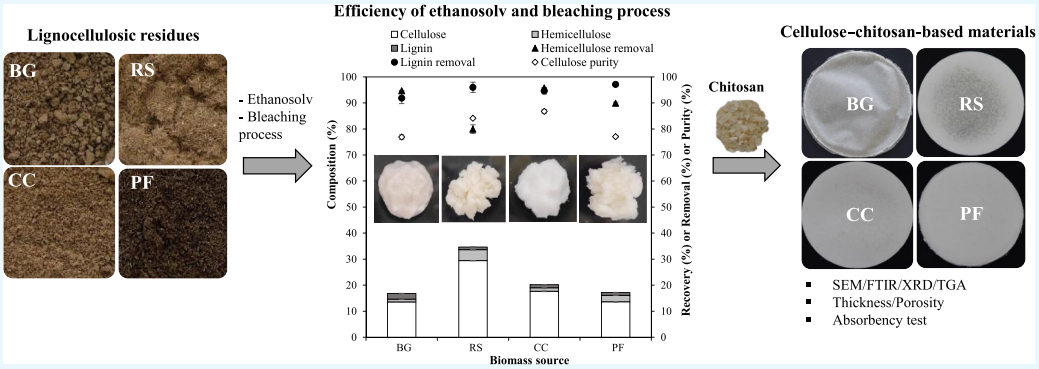

ABSTRACT: Cellulose-based composites are promising biomaterials with potent applications in absorbents, cosmetics, and healthcare industries. In this study, the cellulose fractions from various agricultural residues, including bagasse (BG), rice straw (RS), corncob (CC), and palm fiber (PF), were prepared by the organosolv process using 70% v/v ethanol, followed by bleaching and forming with chitosan powder. Organosolv treatment at 180 °C of BG, RS, and PF and at 190 °C of CC for 60 min using H_2SO_4 as the catalyst was optimal for high cellulose recovery (87.9−98.9%) with efficient removals of the hemicellulose (59.3−86.0%) and lignin (61.1−73.7%). High cellulose purity in the solids (76.9−86.8%) was obtained after bleaching with 4% v/v H_2O_2 compared with that of 84.9% for commercial cellulose. The isolated celluloses were incubated with 2% w/v chitosan solution in acetic acid for the formation of the hydrogen-bonding interaction between the cellulose fiber and chitosan. The pieces of evidence of the obtained sheet materials were characterized by scanning electron microscopy, Fourier-transform infrared spectroscopy, X-ray diffraction analysis, and thermogravimetric analysis. All cellulose−chitosan materials absorbed water fraction in the range of 54.3−94.2 g/m^2. Efficient oil absorption was observed for cellulose−chitosan sheets prepared from PF (96.3 g/m^2) and CC (81.1 g/m^2). This work demonstrated the preparation of potent biobased absorbents with a promising application in waste treatment and healthcare industries.

1. INTRODUCTION

Cellulose is a polymeric highly crystalline structure composed of linear chains of polysaccharide of D-glucose monomers which are linked together by β-1,4-glycosidic bonds. It is an abundant natural polymer with advantageous properties including its biodegradability and recyclability which make cellulose an eco-friendly material with various applications. Lignocellulosic plant biomass is the main source of cellulose which can be further converted into fuels, chemicals, and materials. The annual production of lignocellulosic residues from forestry and agricultural residues worldwide was 181.5 billion tons.[1] Cellulose content in agricultural wastes is in the range of 35−50%, while the rest comprises hemicellulose (20−35%) and lignin (10−20%), which are associated together in the form of a complex lignocellulosic structure.[2] Several chemical and thermochemical pretreatment methods, for example, liquid hot water, diluted acid alkaline, and organosolv processes, are interestingly attractive for separating the cellulose fraction from various lignocellulosic materials[3] with variation in specificity toward the removal of noncellulose

Received: June 15, 2021
Accepted: July 30, 2021
Published: August 23, 2021

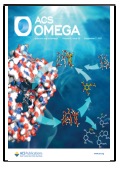

Table 1. Chemical Compositions of Different Lignocellulosic Biomasses on a Dry Weight Basis

	composition (%)				
lignocellulosic biomass	cellulose	hemicellulose	lignin	ash	Extractives
BG	29.3 ± 0.1	19.7 ± 0.5	27.2 ± 4.9	7.4 ± 0.0	16.4 ± 4.2
RS	37.5 ± 0.0	20.9 ± 1.7	24.9 ± 1.7	6.2 ± 0.2	10.6 ± 0.6
CC	37.5 ± 0.3	32.4 ± 1.1	21.6 ± 0.0	2.0 ± 0.0	6.6 ± 0.4
PF	27.0 ± 2.2	24.5 ± 0.6	38.1 ± 5.7	3.5 ± 0.3	6.9 ± 0.8

components using different mechanisms. This results in the enrichment of the cellulose fraction with a higher susceptibility to subsequent enzymatic processing.[4]

Organosolv is an efficient process which uses organic solvents, mostly alcohols (methanol, ethanol, ethylene glycol, and glycerol) and organic acids (acetic acid and formic acid), for the pretreatment of lignocellulosic materials.[5] This method offers high efficiency on lignin solubilization, resulting in the preparation of a cellulose fraction with high purity. The solvent can be simply recovered and recycled using distillation methods.[6] Among various solvents, ethanol is the most widely used solvent in organosolv, and the process, called ethanosolv, is advantageous due to its high delignification efficiency with the nontoxic nature and easy recovery of ethanol.[6] The isolated lignin from the organosolv process offers high purity with a trace sugar contamination, a good solubility in many organic solvents, and low molecular weight. Organosolv lignin can be used as starting materials or additives in many applications such as preparation of phenolic compounds,[7] polymeric materials (phenolic powder resins, polyurethane, and epoxy resins),[8] and carbon fiber.[9] The process usually operates with 25−75% v/v ethanol under the temperature range of 140−220 °C for 30−240 min.[2,6,10] However, the suitable operating conditions with the balance on economic feasibility of the ethanosolv process need to be optimized for individual biomass and the setup of operating machines. The enriched cellulose fraction is further bleached using various chemicals, for example, chlorine-based (NaClO and ClO_2) and the more-eco-friendly peroxide-based agents such as H_2O_2.[11] This leads to the removal of the residual lignin to obtain cellulose fibers with high brightness. The obtained cellulose fibers are odorless, tasteless, insoluble in water, and organic solvents with conserved inter-/intramolecular hydrogen bonds and van der Waals forces in the structure, which can be used for various applications.

The cellulose-based material is a promising three-dimensional network of structural polymer containing numerous hydrophilic hydroxyl groups, making it potent for water absorption by trapping water inside the structure.[12] The cellulose-based absorbents are used in various applications such as smart materials, waste treatment, healthcare and hygienic products, agricultural materials, and textiles.[12] Other natural polymers, such as chitosan which is obtained from the partial deacetylation of chitin isolated from crustaceans and insects, also possess absorbent property by interacting with its amine groups.[13] Chitin also possesses antimicrobial activity, biocompatibility, and biodegradability properties desirable for application in medical fields. Interestingly, the polymeric material formed between cellulose and chitosan has been shown to improve the performance on absorption due to the increasing capability to absorb water and the stability of its structure.[14] It was then applied in various fields such as tissue engineering, drug delivery, wound dressing, and metal absorbent.[13,15]

In this work, the preparation of cellulose fibers from different potent agricultural wastes including bagasse (BG), rice straw (RS), corncob (CC), and palm fiber (PF) using an ethanosolv process was studied. The pretreated cellulose-enriched fractions were bleached by hydrogen peroxide and formed with chitosan. The cellulose−chitosan materials or sheets were characterized for absorption property and physical characteristics by different techniques [scanning electron microscopy (SEM), Fourier-transform infrared (FTIR) spectroscopy, X-ray diffraction (XRD) analysis, and thermogravimetric analysis (TGA)] compared to the composite material obtained from commercial cellulose and chitosan. This work provides insights into the property of the cellulose−chitosan-based materials and potential for further industrial applications.

2. RESULTS AND DISCUSSION

2.1. Ethanosolv Pretreatment of Different Lignocellulosic Biomasses. All raw materials used in this study showed good homogeneity as preliminarily observed from their physical appearance (Figure 2) prior to the chemical composition analysis. This resulted from the biomass physically processed and sieved to a specific size range. According to the chemical composition analysis, RS and CC contained the highest cellulose content of higher than 37.5%, followed by BG (29.3%) and PF (27.0%), respectively. The hemicellulose and lignin contents were in the ranges of 19.7−32.4 and 21.6−38.1% (w/w) on a dry weight basis, respectively, as listed in Table 1. The minor ash content and the extractive fraction containing starch, wax, syrup, organic acids, and the soluble protein were in ranges of 2.0−7.4 and 6.6−16.4% (w/w), respectively.

In the organosolv pretreatment, the use of ethanol as an organic solvent in the presence of an acid catalyst showed major effects on the solubilization of hemicellulose and lignin from the biomass due to cleavages of internal ether bond in lignin and the intermolecular lignin−hemicellulose bond.[16] The efficiency of the organosolv process depends on the type of solvents, the operating conditions, and the nature of the raw materials.[16] However, the reaction temperature represented one of the most influencing factors on the ethanosolv pretreatment of biomass reported by previous studies.[17,18] Therefore, the fractionation of cellulose fractions from various lignocellulosic residues in this work focused on studying the effect of the reaction temperature on fixing the other reaction parameters in the organosolv process. The effects of reaction temperature in the range of 160−190 °C were studied in the ethanosolv pretreatment of various biomasses using 70% aqueous ethanol for 60 min with an addition of 1% w/w H_2SO_4 as an acid catalyst. The process efficiency in terms of pulp yield, cellulose recovery, along with the hemicellulose and lignin removals in ethanosolv pretreatment is shown in Figure 1. Increasing the temperature from 160 to 190 °C showed increasing trends of hemicellulose and lignin solubilization into the solvent phase along with the lower pulp yield in the range

https://doi.org/10.1021/acsomega.1c03141
ACS Omega 2021, 6, 22791−22802

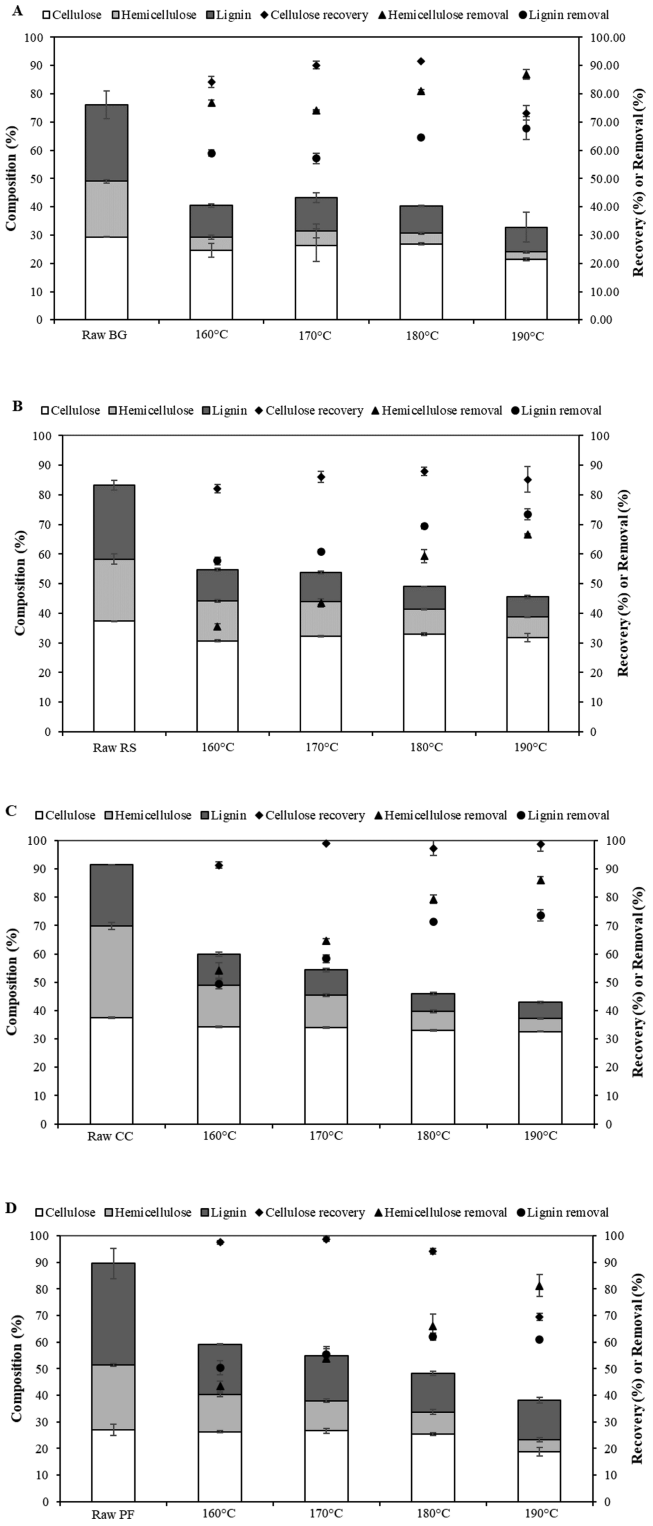

Figure 1. Effects of organosolv pretreatment at different temperatures on the chemical composition of different raw materials: (A) BG, (B) RS, (C) CC, and (D) PF. The reaction contained 10% (w/v) biomass in a ratio of 70% aqueous ethanol with 1% w/w H_2SO_4 with stirring at 400 rpm for 60 min.

of 64.2−40.2% on the weight basis, leading to the enrichment of cellulose in the solid fractions. Partial removals of the noncellulosic components were in the range of 35.6−87.0% for hemicellulose and 49.4−73.7% for lignin for all the studied raw materials. The highest cellulose recoveries of 91.6 and 87.9% were achieved for BG and RS, respectively, at 180 °C, while the highest recoveries of 99.0 and 98.7% were obtained for CC and PF at 170 °C, respectively. The reaction temperature at 190 °C gave the highest removal efficiencies on hemicellulose and lignin with 66.6−87.0 and 61.1−73.7%, respectively, for different raw materials. The trends observed on the effect of reaction temperature agree well with those reported in the previous work, suggesting that the increase of temperature led to the increasing removal of the noncellulosic components. For example, the previous study reported that the ethanosolv pretreatment of corn straw using the mixture of 75% aqueous ethanol in the presence of an acid catalyst and H_2O_2 as an oxidizing agent in the temperature range of 100−160 °C led to increasing hemicellulose and lignin removals in the ranges of 38.5−100.0 and 68.0−99.6%, respectively.[19]

Among delignification from different lignocellulosic residues under the experimental condition, the higher lignin removal efficiencies with 73.7 and 73.4% were observed from CC and RS compared to other pretreated biomass of BG and PF with 67.8 and 61.1%, respectively, after the ethanosolv process at 190 °C. According to the high cellulose recovery with high removal efficiencies of hemicellulose and lignin, the solid fractions obtained at 180 °C for BG, RS, and PF and 190 °C for CC were considered optimal conditions and used for the preparation of the cellulose fractions in subsequent experiments.

2.2. Bleaching of the Cellulose Pulps. After the ethanosolv pretreatment, the solid pulps isolated from different biomasses under the respective optimal conditions were bleached using H_2O_2 under alkaline conditions to further remove the residual lignin and associated hemicellulose. Hydrogen peroxide (H_2O_2) is commonly used as an oxidative agent in the paper industry. The alkaline hydrogen peroxide (AHP) process led to efficient delignification by cleaving the lignin structure, which also resulted in the partial removal of hemicellulose associated with lignin.[20,21] Remarkable increases in the whiteness of the pulps were observed for all lignocellulosic biomass after the bleaching step (Figure 2). This bleaching agent under alkaline conditions resulted in the generation of oxidative radicals, especially perhydroxyl anion (HOO^-), which led to the oxidation of the quinone structure in lignin to low-molecular aliphatic compounds and the chromophore structure of lignin at carbonyl groups involved in the color change.[22,23] Additionally, H_2O_2 affected the interruption of the conjugated double bonds in the lignin structure, which resulted in altering the dark brown color of lignin to colorless.[24] Removal of lignin by bleaching led to the enrichment of the cellulose fraction and increased brightness, as shown in Figure 3. The bleached pulps showed a high cellulose purity (76.9−86.8%) compared to the raw materials (27.0−37.5%). The hemicellulose and lignin contents were decreased to 1.1−4.2 and 1.0−2.2%, respectively, equivalent to the total hemicellulose and lignin removal of 79.9−95.8 and 91.8−97.1%, respectively, compared to the raw materials. The purity of cellulose achieved was similar to that of the commercial grade cellulose (84.9%), which contained the hemicellulose and lignin fraction with 12.2 and 2.8%, respectively. The results on cellulose purity and removal of hemicellulose and lignin in our study were correlated to several previous works using H_2O_2 as a green agent both in the bleaching and pretreatment process.[25−28] This led to the increasing efficiency of the lignin and hemicellulose removal and safety compared to the use of toxic chlorine-based

https://doi.org/10.1021/acsomega.1c03141
ACS Omega 2021, 6, 22791−22802

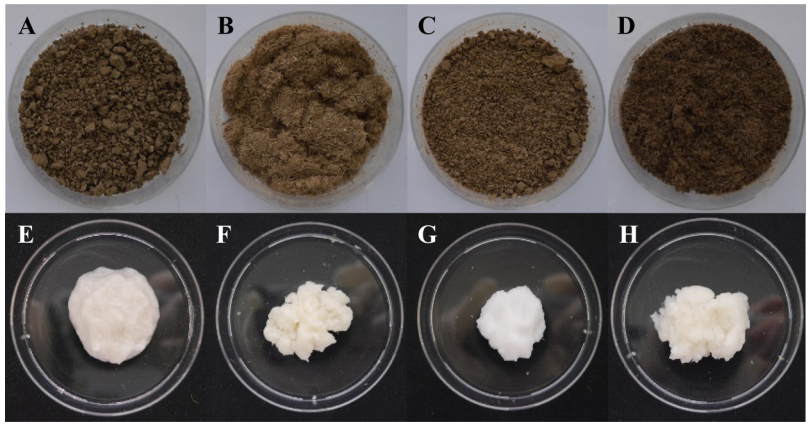

Figure 2. Illustration of cellulose pulps from different raw materials before and after bleaching: (A) BG, (B) RS, (C) CC, (D) PF, (E) bleached BG, (F) bleached RS, (G) bleached CC, and (H) bleached PF.

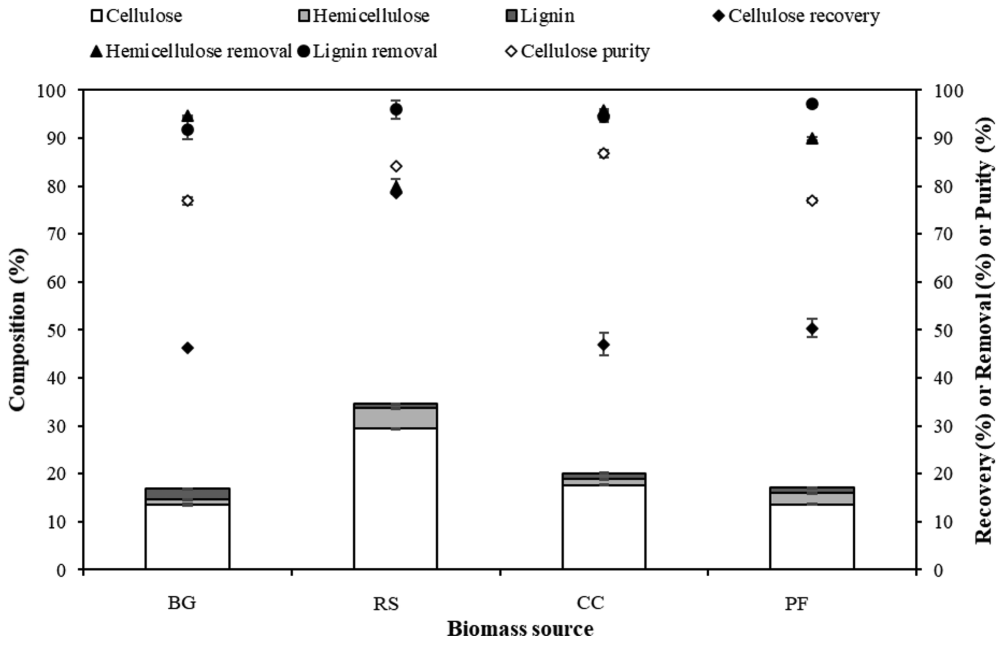

Figure 3. Effects of bleaching on chemical compositions of the cellulose pulps from different raw materials pretreated by the organosolv process at the optimized reaction temperature. The organosolv cellulose pulps were bleached by 4% v/v H_2O_2 at pH 11.5 adjusted by NaOH and incubated at 80 °C for 6 h.

chemicals. The previous study reported that the H_2O_2 bleaching treatment on the wood samples under 6% H_2O_2 with 1% NaOH and trisodium citrate dihydrate at 60 °C for 2.5 h resulted in 8.7 and 38.7% of hemicellulose and lignin removals.[22] In addition, the AHP pretreatment of sugarcane BG, oil palm mesocarp fiber, and corn stover at different reaction conditions demonstrated in the range of cellulose purity (58.1−65.9%), hemicellulose removal (19.8−84.7%), and lignin removal (17.6−78.6%), respectively.[25−27] Later, the bleached cellulose pulps were then used for the subsequent preparation of cellulose−chitosan materials in the next step.

2.3. Physicochemical Characterization of Cellulose−Chitosan Materials. *2.3.1. Physical Appearance and SEM Analysis.* The cellulose−chitosan-based materials prepared from all lignocellulosic biomasses were formed as thin nontransparent sheets with white color similar to the sample prepared from the commercial cellulose (Figure 4). The physical characteristics of the cellulose−chitosan composites were different from the chitosan sheet, which was formed as a

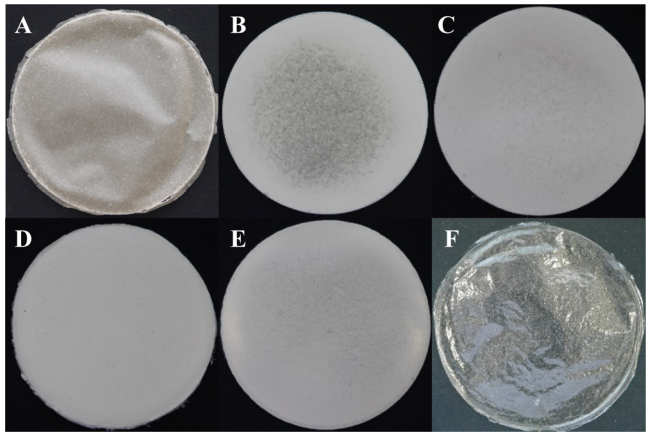

Figure 4. Illustration of cellulose−chitosan-based materials: (A) BG sheet, (B) RS sheet, (C) CC sheet, (D) PF sheet, (E) commercial cellulose sheet, and (F) chitosan sheet.

https://doi.org/10.1021/acsomega.1c03141
ACS Omega 2021, 6, 22791−22802

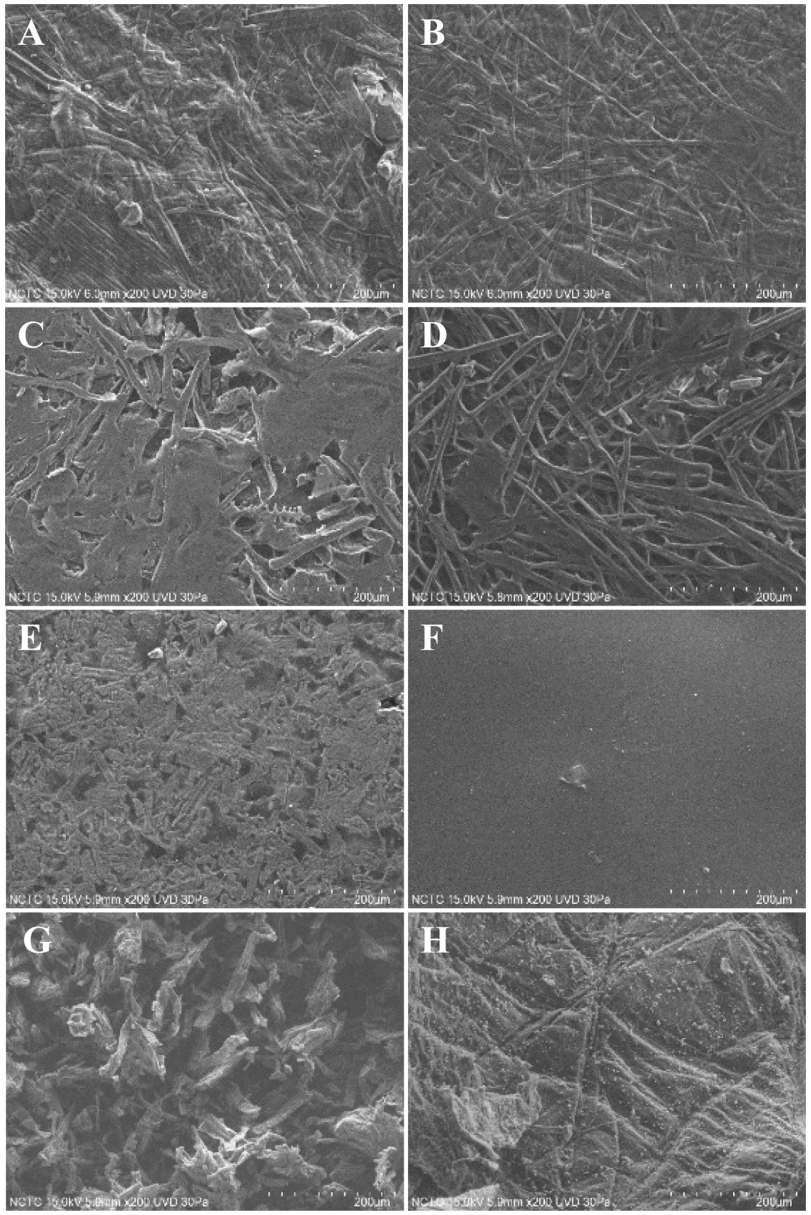

Figure 5. SEM analysis of cellulose−chitosan-based materials compared to the commercial cellulose and chitosan powder: (A) BG sheet, (B) RS sheet, (C) CC sheet, (D) PF sheet, (E) commercial cellulose sheet, (F) chitosan sheet, (G) commercial cellulose powder, and (H) chitosan powder.

thin and fragile transparent film. Later, the morphology and structure of all cellulose−chitosan-based materials were analyzed by SEM (Figure 5). It was found that the RS and PF sheets contained the long crisscross fiber formed similar to small tree branches, while the BG and CC sheets contained a dense fiber structure with various lengths such as small flakes with short branches and rough flat pieces. The commercial cellulose sheet showed a nonfibrous and flat structure, while the commercial chitosan sheet and powder presented a nonporous and smooth structure. All cellulose−chitosan-based materials prepared from the biomass showed more branched-fibrous network structures, especially the RS and PF sheets, resulting in more porosity and structural connection compared to the sheet material prepared from the commercial cellulose. The results suggested that the ethanosolv process developed in this study can be used to prepare the cellulose fibers with low damage to the cellulose structure and efficient removal of the hemicellulose and lignin. This corresponded to the previously reported pretreatment of biomass by the organosolv process, which led to high cellulose recovery in the solid fraction and more efficiency of hemicellulose and lignin solubilization compared to the other pretreatment methods.[8] The structures of sheet materials observed was similar to those reported from previous works.[29−31] According to previous SEM analysis, it was found that the paper sheets prepared from bleached BG and RG pulps presented the dense fiber with the short branch structure and long crisscross fiber, respectively.[31] A fiber structure with small pores was shown from the paper-based bacterial cellulose−chitosan nanocomposites.[29] Besides, the structure of the chitosan membrane obtained from mixing with 1% v/v acetic acid also appeared with a smooth flat surface structure and no pores.[30]

2.3.2. Thickness Analysis. The thickness and porosity of PF, CC, RS, and BG sheets varied between 0.178 and 0.385 mm

https://doi.org/10.1021/acsomega.1c03141
ACS Omega 2021, 6, 22791−22802

and 12.7−79.7%, respectively (Table 2). The PF sheet showed the highest thickness with 0.385 and contained the highest porosity of 79.7%, while the low thickness of the BG sheet was observed with the minimum porosity of 12.7% compared to the commercial cellulose sheet with a thickness of 0.193 mm and a porosity of 51.2%. No porosity was observed from the chitosan sheet. Increasing thickness of the cellulose−chitosan sheets was found to be related to their increasing porosity due to the space formation during the cellulose−chitosan-based material preparation step, resulting in a swollen structure with high porosity. This porous structure of the cellulose−chitosan sheets prepared from different biomasses corresponded to the SEM analysis which showed more branched-fibrous structures and pores from PF, CC, and RS as feedstocks, respectively. The observed thickness of the cellulose−chitosan sheets observed in this work was in the same range to those prepared from cellulose−chitosan nanocomposite, cellulose nanofibril, cellulose hydrogel derived from palm oil trunk, and bacterial cellulose membrane from *Acetobacter xylinum,* which were in the range of 0.060−0.540 mm.[29,32−34]

Table 2. Thickness and Porosity of the Cellulose−Chitosan-Based Materials[a]

samples	thickness (mm)	porosity (%)
BG sheet	0.178 ± 0.005	12.7 ± 2.4
RS sheet	0.251 ± 0.026	55.2 ± 4.7
CC sheet	0.266 ± 0.013	61.3 ± 1.8
PF sheet	0.385 ± 0.035	79.7 ± 1.9
commercial cellulose sheet	0.193 ± 0.010	51.2 ± 2.4
chitosan sheet	0.065 ± 0.006	ND

[a]ND: not detectable.

2.3.3. Absorbent Efficiency Analysis. Generally, the absorbent material prepared from cellulose fibers can effectively absorb water by interactions between the hydroxyl groups of the fibers and water molecules.[35] The amorphous regions of cellulose together with the free spaces between the noncrystalline hemicellulose led to the swelling property and water retention of cellulose-based materials.[36] Apart from the hydroxyl groups of cellulose, the amine groups of chitosan are also good hydrophilic sites for water uptake.[37] The water absorption efficiency of cellulose−chitosan sheets prepared from biomass in this study was in the range of 54.3−94.2 g/m^2 (Figure 6), which were correlated to the increase in porosity of the sheet materials. However, the water absorption of the commercial cellulose sheet with 54.8% was rather lower than the cellulose−chitosan materials prepared from RS, CC, and PF due to less hydrophilic sites and porosity characteristic. The oil absorption efficiencies of 96.3 and 81.1 g/m^2 were observed only for PF and CC sheets. The ability on oil absorption was related to the hydrophobic surfaces, porosity, and interconnected pores of the materials.[38] The PF and CC sheets presented very high porosity which potentially led to their high absorption of oil on the hydrophobic sites in these materials. Variation in the oil adsorption efficiency was previously reported for different cellulose-based materials, for example, cellulose nanofibril−polyvinyl alcohol microspheres, cellulose hydrogel, and cellulose nanofibril aerogel.[38−40]

2.3.4. FTIR Analysis. The functional group profiles of cellulose−chitosan-based sheets, commercial cellulose, and chitosan powder were determined by FTIR analysis (Figure 7 and Table 3). The FTIR spectra of commercial cellulose showed signature peaks at 3341.58 cm^{-1} for O−H stretching, 2904.27 cm^{-1} for C−H stretching of CH_2, 1643.70 cm^{-1} for O−H bending, 1371.42 cm^{-1} for C−H bending, and 1161.46 cm^{-1} for C−O−C stretching, corresponding to the spectra band of cellulose previously reported by Kwon et al. (2020) and Wahid et al. (2019).[41,42] The specific absorption peaks at 1655.81 and 1573.09 cm^{-1} of C═O stretching from amide I and N−H bending were observed from the pure chitosan powder,[43] while the sheet sample prepared from pure chitosan showed the peak of C═N stretching of the amine group at 1556.26 cm^{-1}, suggesting the internal linkage between each chitosan molecule.[44] All cellulose−chitosan sheets obtained from various lignocellulosic biomasses demonstrated the signature peaks present in both commercial cellulose and chitosan. The detail in the formation of the hydrogen-bonding interaction between cellulose and chitosan from BG, RS, CC, and PF sheets was observed from the lower intensity of O−H bending compared with commercial cellulose containing the high intra- and intermolecular hydrogen bonds with abundant hydroxyl groups. This result of hydrogen-bonding formation observed corresponded to previously reported results for bacterial cellulose−chitosan hydrogel[42] and semi-IPN superabsorbent chitosan−starch hydrogel.[45] Besides, the lower intensity of C−H stretching of CH_2 from all cellulose−chitosan samples was observed compared to commercial cellulose, which could be due to the lower methylene group after the formation of cellulose−chitosan sheets.

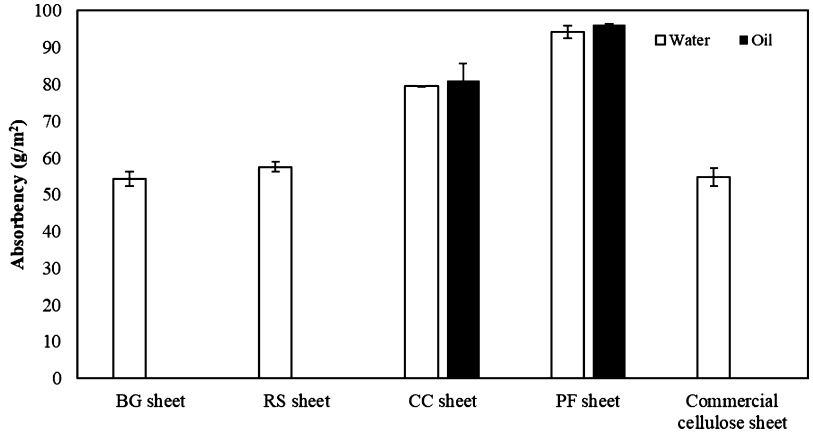

Figure 6. Water and oil absorbency of cellulose−chitosan-based materials prepared from different raw materials and commercial cellulose.

https://doi.org/10.1021/acsomega.1c03141
ACS Omega 2021, 6, 22791−22802

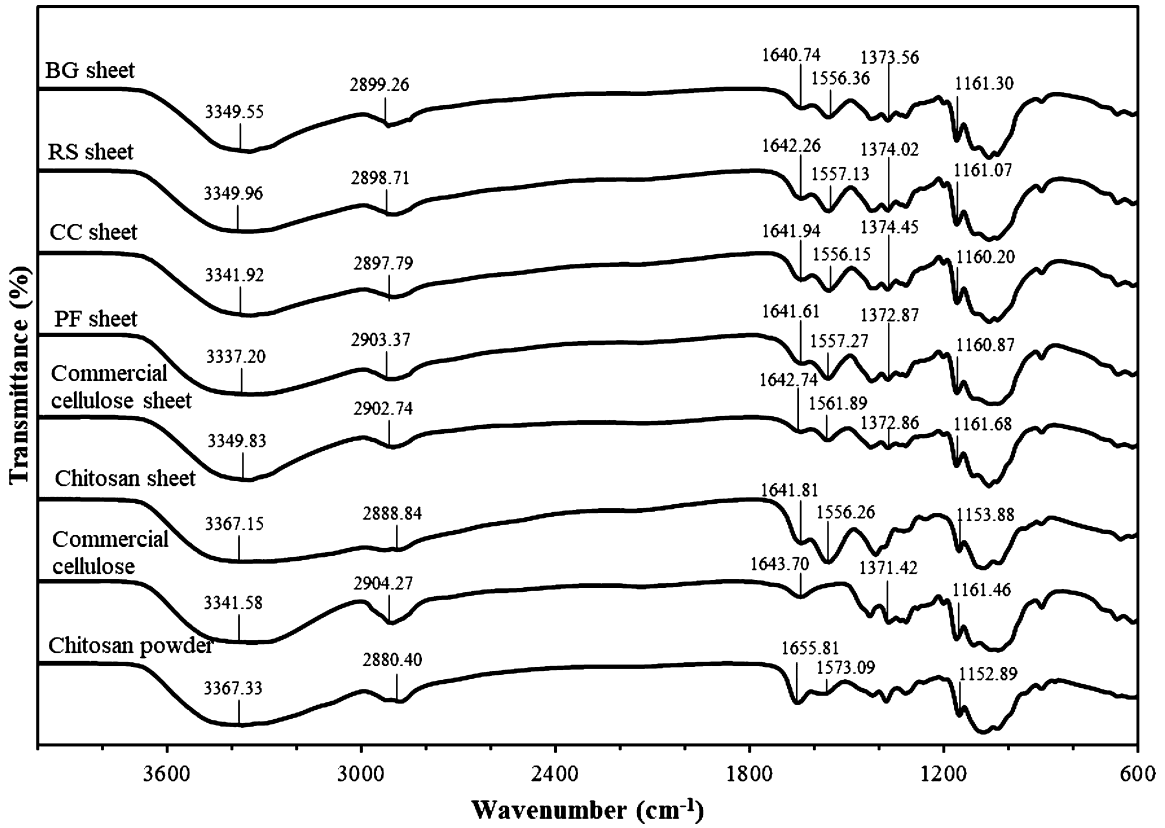

Figure 7. FTIR spectra of cellulose−chitosan-based materials compared to the commercial cellulose and chitosan powder.

Table 3. FTIR Analysis of the Cellulose−Chitosan-Based Materials Compared to the Commercial Cellulose and Chitosan Powder

	wavenumber (cm^{-1}) of the functional group							
sample	O−H stretching	C−H stretching	C=O stretching	O−H bending	N−H bending	C=N stretching	C−H bending	C−O−C stretching
BG sheet	3349.55	2899.26		1640.74		1556.36	1373.56	1161.30
RS sheet	3349.96	2898.71		1642.26		1557.13	1374.02	1161.07
CC sheet	3341.92	2897.79		1641.94		1556.15	1374.45	1160.20
PF sheet	3337.20	2903.37		1641.61		1557.27	1372.87	1160.87
commercial cellulose sheet	3349.83	2902.74		1642.74		1561.89	1372.86	1161.68
chitosan sheet	3367.15	2888.84		1641.81		1556.26		1153.88
commercial cellulose	3341.58	2904.27		1643.70			1371.42	1161.46
chitosan powder	3367.33	2880.40	1655.81		1573.09			1152.89

2.3.5. XRD Analysis. The microstructures of cellulose−chitosan sheets, commercial cellulose, and chitosan powder were analyzed by XRD (Figure 8). It was found that all sheet materials and the commercial cellulose showed the two main XRD peaks approximately at $2\theta \approx 15$ and 22° corresponding to (110) and (200) planes, respectively, which are attributed to the typical cellulose I structure.[46−48] Especially, the XRD pattern of all cellulose−chitosan sheet samples demonstrated these lower intensity peaks compared to the commercial cellulose powder. This could be due to the decline in the free hydroxyl group (OH group) resulted from the formation of hydrogen-bonding interactions between the cellulose and chitosan structure corresponding to the lower FTIR absorption of O−H bending from all cellulose−chitosan sheets. Meanwhile, the chitosan sheet showed no significant crystalline peak due to the internal linkage of the chitosan molecule similar to the chitosan film and hydrogel previously reported by Cervera et al. (2004) and Wahid et al. (2019).[42,49] The chitosan powder presented two different broad peaks at $2\theta = 9.50$ and 19.74° referred to the semicrystalline structure from strong intra- and intermolecular interactions of hydrogen bonds formed among amine, alcohol, and other functional groups present in the chitosan molecule.[30]

In addition, the decrease in the intensity of the crystalline structure in the XRD pattern was related to the lower crystallinity index of all sheet materials with the range from 43.3 to 51.0% when compared to 65.7% of the commercial cellulose (Table 4). It indicated that the formation of hydrogen bonding between cellulose and chitosan led to the decline in the crystallinity index. Besides, this lower crystallinity index correlated to the absorbency test that showed the increase in the water absorption efficiency of the PF, CC, and RS sheets, resulting in more swelling and water retention from the high amorphous regions of the materials.

https://doi.org/10.1021/acsomega.1c03141
ACS Omega 2021, 6, 22791−22802

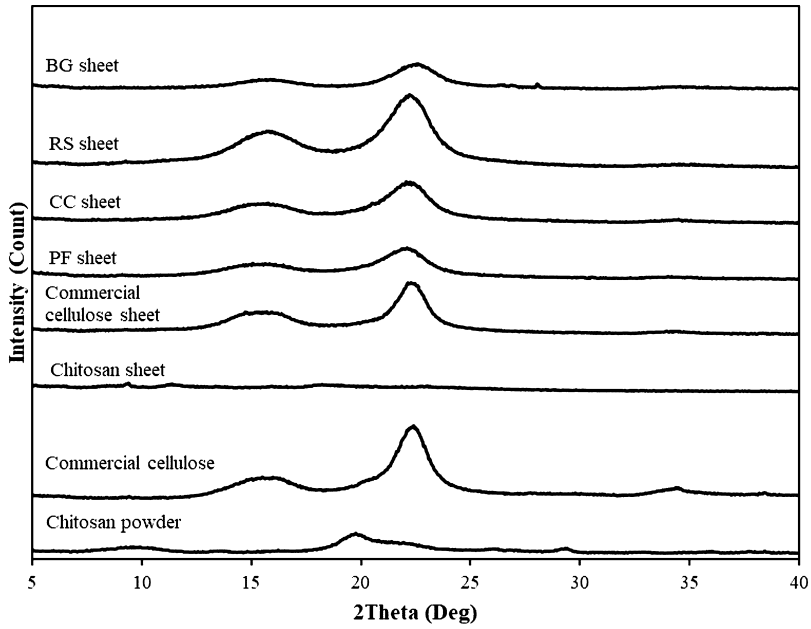

Figure 8. XRD patterns of cellulose−chitosan-based materials compared to the commercial cellulose and chitosan powder.

Table 4. Crystallinity Index of the Cellulose−Chitosan-Based Materials Compared to the Commercial Cellulose and Chitosan Powder[a]

sample	crystallinity (%)
BG sheet	51.0
RS sheet	47.0
CC sheet	45.9
PF sheet	43.3
commercial cellulose sheet	52.2
chitosan sheet	ND
commercial cellulose	65.7
chitosan powder	52.6

[a]ND: not detectable.

2.3.6. Thermal Analysis. The thermal property of all cellulose−chitosan-based materials prepared from various biomasses was characterized by the TGA technique. The results were compared with the commercial cellulose, chitosan sheet, and chitosan powder (Figure 9). The TGA thermogram at 30−900 °C of all samples demonstrated the single step thermal degradation pattern. The TGA curve of the chitosan sheet was sharply higher with thermal degradation at 180 °C, while the other samples were initially decomposed in the range of 200−350 °C. Its degradation at lower temperatures could be due to the change in the ordered structure after the formation of the chitosan sheet corresponding to no observation in the crystalline peak from XRD analysis. The weight loss starting at around 250 and 230 °C was observed for the commercial cellulose sheet and chitosan sheet, respectively, similar to the

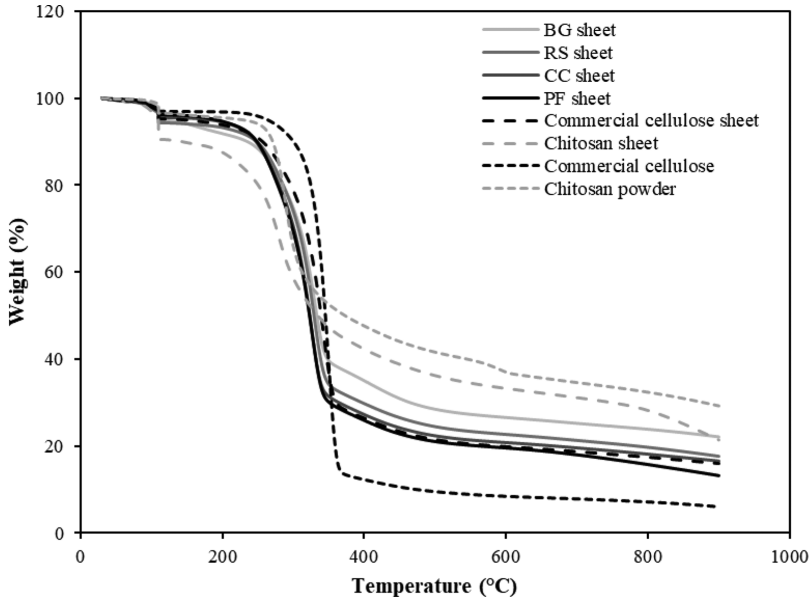

Figure 9. TGA thermograms of cellulose−chitosan-based materials compared to the commercial cellulose and chitosan powder.

https://doi.org/10.1021/acsomega.1c03141
ACS Omega 2021, 6, 22791−22802

decomposition of the cellulose−chitosan-based composition, as reported in previous works.[50,51] The TGA degradation pattern of all cellulose−chitosan sheets prepared from biomass and commercial cellulose were obviously decreased from 200 to 380 °C with the range of weight loss from 5 to 71%. At the temperature higher than 400 °C, the lowest remaining weight of commercial cellulose with <10% was observed, while the other samples gave the residues ranging from 13 to 29%.

The chitosan powder and sheet showed the higher residues compared to all cellulose−chitosan-based sheets due to the impurity of the other contaminations in chitosan such as protein and ash.[52] According to the results, the commercial cellulose presented the highest thermal stability and degradation, resulting in higher molecular weight and crystallinity index with less contaminated substances in the chemical structure.[53] It indicated that the higher thermal stability correlated to the increase in the crystallinity index and high intensity of O−H bending analyzed by XRD and FTIR analysis, respectively. Moreover, the thermal stability of all cellulose−chitosan sheets prepared from different sources was comparable to the samples prepared from commercial cellulose. The residues of all sheet materials at a temperature higher than 400 °C presented the weight loss in between the commercial cellulose and chitosan, suggesting the formation of a hydrogen-bonding interaction between cellulose and chitosan in the sheet materials.

3. CONCLUSIONS

In this work, the ethanosolv pretreatment with subsequent H_2O_2 bleaching was applied to provide the enriched cellulose fraction with high purity for the preparation of the cellulose−chitosan materials. Formation of the hydrogen-bonding interaction between cellulose and chitosan was confirmed by FTIR, XRD, and TGA. The cellulose−chitosan materials prepared from different biomasses showed high performance on water absorption ranked from PF > CC > RS > BG sheets, while PF and CC sheets were capable on oil absorption, which were relevant to their physical properties, for example, porosity and thickness of the material structure. Moreover, the higher water absorption by the prepared sheet materials was found to correspond to the decline in the crystallinity index with lower XRD peaks of the cellulose structure and thermal stability. Interestingly, the PF and CC sheets could be good candidates when used as absorbents in waste treatment and healthcare industries,[13,15] as reflected by their properties. This work provided the simple preparation method for the cellulose−chitosan-based materials derived from local agricultural biomass for further potential applications.

4. MATERIALS AND METHODS

4.1. Materials. Sugarcane BG was kindly provided by Mitr Phol Sugar Mill (Chaiyaphum, Thailand). RG was obtained from a local farm in Pathum Thani Province, Thailand. CC was provided by an animal farm in Phetchabun Province, Thailand. PF was obtained from Suksomboon Palm Oil Industry, Songkla, Thailand. All of the biomasses were milled using a cutting mill (Retsch ZM2000, Retsch GmbH, Haan, Germany) and sieved to the size between 0.425 and 1 mm. The raw materials were analyzed for the chemical compositions following the National Renewable Energy Laboratory (NREL) method.[54] Chitosan powder (M_w = 5.4 × 10^4 Da) was purchased from Sinudom Agriculture Products Ltd., Part (Surat Thani, Thailand). Commercial cellulose (CAS no. 9004-34-6) was purchased from HIMEDIA (Mumbai, India). Soybean oil was obtained from a local market (Angoon brand, Thai Vegetable Oil PCL, Nakorn Pathom, Thailand). Chemicals and reagents were of analytical grade obtained from major chemical companies (Sigma, Merck, and Fluka).

4.2. Ethanosolv Pretreatment. The pretreatment process was performed in a 1 L reactor (Parr Instruments 4520, Moline, USA). The reactions contained 10% solid loading of the raw material in 70% v/v aqueous ethanol in the presence of 1% w/w sulfuric acid (H_2SO_4) and the initial pressure of 5 bars by nitrogen gas. The reactions were operated at 160−190 °C for 60 min with stirring at 400 rpm. The reactions were immediately quenched in an ice bath to cool down the reactions. The cellulose-enriched fractions were separated from the liquid phase by suction through a filter paper (Whatman no. 4) and dried overnight for removing at 70 °C before the calculation of pulp yield (eq 1). The pretreatment conditions were evaluated based on cellulose recovery (eq 2), hemicellulose removal (eq 3), and lignin removal (eq 4). The chemical compositions of the pretreated biomass were analyzed by the standard NREL method.

$$\%\ \text{Pulp yield} = \left(\frac{\text{final solid pulp weight (g)}}{\text{initial biomass weight (g)}} \times 100\right) - \%\ \text{moisture content} \quad (1)$$

$$\%\ \text{cellulose recovery} = \frac{\text{final cellulose content (g)}}{\text{initial cellulose content (g)}} \times \%\ \text{pulp yield} \quad (2)$$

$$\%\ \text{hemicellulose removal} = \frac{(\text{initial content} - \text{final content})_{\text{hemicellulose}}\ (\text{g})}{(\text{initial content})_{\text{hemicellulose}}\ (\text{g})} \times \%\ \text{pulp yield} \quad (3)$$

$$\%\ \text{lignin removal} = \frac{(\text{initial content} - \text{final content})_{\text{lignin}}\ (\text{g})}{(\text{initial content})_{\text{lignin}}\ (\text{g})} \times \%\ \text{pulp yield} \quad (4)$$

4.3. Cellulose Bleaching by H_2O_2 Treatment. The solid pulps of each biomass obtained under the optimal conditions were bleached using H_2O_2 treatment according to the method modified from Mussatto et al., 2008.[55] The reactions contained 5% (w/v) dried solid pulp with 4% v/v H_2O_2 with pH adjusted to 11.5 by NaOH and then treated at 80 °C for 6 h. A fresh H_2O_2 solution was added to the reactions to 4% v/v H_2O_2 every 2 h. The solid fraction was collected by filtering through a 0.045 mm sieve before washing with distilled water to neutral pH and then kept at 4 °C before further use. The chemical compositions were analyzed by the NREL method. The percentage of cellulose purity was obtained from the cellulose content in the solid fraction after the bleaching process.

4.4. Preparation of Cellulose−Chitosan-Based Materials. The chitosan solution was prepared by mixing 2% w/v chitosan in 2% v/v acetic acid using a homogenizer (DLAB D500, Beijing, China) and then heated at 100 °C with stirring for 2 h. The chitosan solution was collected after centrifugation

https://doi.org/10.1021/acsomega.1c03141
ACS Omega 2021, 6, 22791−22802

at 4000 rpm for 20 min. Next, 6 g of bleached cellulose samples from different biomasses was added to 100 mL of the chitosan solution and thoroughly mixed by a homogenizer and then stirred at 100 °C for 30 min. The obtained solution (10 mL) was poured in plastic Petri dishes and left at room temperature until completely dried. All sheet materials prepared from different biomasses were compared with that from the commercial cellulose.

4.5. Sugar Analysis. The sugar profiles (glucose, xylose, and arabinose) after biomass composition analysis by the NREL method were analyzed by a high-performance liquid chromatograph (SPD-M10A DAD, Shimadzu, Kyoto, Japan) equipped with a refractive index detector using an Aminex HPX-87H column (Bio-Rad, Hercules, CA, USA) operating at 65 °C with 5 mM H_2SO_4 as the mobile phase at a flow rate of 0.5 mL/min.

4.6. Characterization of Cellulose−Chitosan-Based Materials. *4.6.1. Scanning Electron Microscopy.* The microstructure and morphology of the cellulose−chitosan-based materials were analyzed by SEM using a FE-SEM SU5000 (Hitachi, Tokyo, Japan). All samples were dried and coated with gold for 50 s according to the standard protocol.[56] An electron beam energy of 5 kV was applied for analysis.

4.6.2. Thickness Measurement. The thickness of the absorbent materials was measured by a micrometer (Mitutoyo 103-137, Kanagawa, Japan). The average thickness of samples was reported from three replicated measurements.

4.6.3. Porosity. The porosity of the samples is calculated according to the equation (eq 5).[57]

$$\varepsilon = \left[1 - \left(\frac{\rho}{a \times \rho_1 + b \times \rho_2}\right)\right] \times 100 \quad (5)$$

where ε is the porosity of the sample (%); a and b are the weight fractions of the actual retained cellulose pulp and chitosan in the absorbent material; and ρ, ρ_1, and ρ_2 are the density of samples, cellulose (1.5 g/cm^3), and chitosan (0.3 g/cm^3), respectively.

4.6.4. Absorbency Test. The absorption efficiency of each cellulose−chitosan material was tested by immersing the material in water or vegetable oil for 5 min at room temperature according to the method modified from Mohamed, El-Sakhawy, and Kamel (2017)[58] The analysis of absorbency was calculated according to eq 6.

$$\text{Absorbency (g/m}^2) = \frac{\text{weight of oil or water drop (g)}}{\text{area of liquid drop (m}^2)} \quad (6)$$

4.6.5. Fourier-Transform Infrared Spectroscopy. The functional groups on cellulose−chitosan-based materials were characterized by FTIR (PerkinElmer System 2000, Waltham, USA) with infrared spectra recorded in the wavenumber range of 600−4000 cm^{-1}. The samples were prepared in potassium bromide (KBr) before examining by using the standard test method ASTM: E1252-98.

4.6.6. XRD Analysis. The crystallinity of cellulose−chitosan-based materials, including commercial cellulose and chitosan, was analyzed by XRD using an X'Pert PRO diffractometer (PANalytical, Almelo, The Netherlands). The samples were prepared to the size of 3 × 3 cm^2 prior to scanning at a speed of 4°/min in the range of 2θ = 5−40° with a step size of 0.04° at 40 kV, 30 mA, and radiation at Cu Kα (λ = 1.54 Å). The crystallinity index was calculated according to eq 7.[59,60]

$$\text{Crystallinity index (\%)} = \left(\frac{I_{002} - I_{am}}{I_{002}}\right) \times 100 \quad (7)$$

where I_{002} is the intensity of the peak for the crystalline portion at 2θ = 20° (chitosan) and 22° (cellulose) and I_{am} is the intensity of the peak for the amorphous portion at 2θ = 10° (chitosan) and 15° (cellulose).

4.6.7. Thermogravimetric Analysis. The thermal stabilities of cellulose−chitosan-based materials, commercial cellulose, and chitosan were analyzed by a Thermogravimetric Analyzer (PerkinElmer Pyris, Waltham, USA) in the temperature range from 30 to 900 °C at a heating rate of 10 °C/min under a helium atmosphere. The temperature condition was raised from 30 to 110 °C and then held at 110 °C for 10 min before increasing the temperature from 110 to 900 °C.

AUTHOR INFORMATION

Corresponding Author

Marisa Raita − *The Joint Graduate School for Energy and Environment (JGSEE), King Mongkut's University of Technology Thonburi, Bangkok 10140, Thailand; BIOTEC-JGSEE Integrative Biorefinery Laboratory, Khlong Luang 12120 Pathumthani, Thailand;* orcid.org/0000-0001-5422-1042; Phone: +66-2117-8032; Email: marisa@jgsee.kmutt.ac.th, marisabkk28@gmail.com

Authors

Suchat Pongchaiphol − *The Joint Graduate School for Energy and Environment (JGSEE), King Mongkut's University of Technology Thonburi, Bangkok 10140, Thailand; BIOTEC-JGSEE Integrative Biorefinery Laboratory, Khlong Luang 12120 Pathumthani, Thailand*

Thanchanok Preechakun − *Biorefinery Technology and Bioproducts Research Group, National Center for Genetic Engineering and Biotechnology (BIOTEC), Khlong Luang 12120 Pathumthani, Thailand; BIOTEC-JGSEE Integrative Biorefinery Laboratory, Khlong Luang 12120 Pathumthani, Thailand*

Verawat Champreda − *Biorefinery Technology and Bioproducts Research Group, National Center for Genetic Engineering and Biotechnology (BIOTEC), Khlong Luang 12120 Pathumthani, Thailand; BIOTEC-JGSEE Integrative Biorefinery Laboratory, Khlong Luang 12120 Pathumthani, Thailand*

Navadol Laosiripojana − *The Joint Graduate School for Energy and Environment (JGSEE), King Mongkut's University of Technology Thonburi, Bangkok 10140, Thailand; BIOTEC-JGSEE Integrative Biorefinery Laboratory, Khlong Luang 12120 Pathumthani, Thailand*

Complete contact information is available at: https://pubs.acs.org/10.1021/acsomega.1c03141

Notes

The authors declare no competing financial interest.

ACKNOWLEDGMENTS

This work was financially supported by the National Science and Technology Development Agency (grant number P-18-51760). Pongchaiphol S. was supported by the Thailand Research Fund (TRF) and Global R&D Co., Ltd. (no.

PHD5910099) under the Research and Researchers for Industries (RRi) project, including the scholarship from The Joint Graduate School of Energy and Environment (JGSEE) (Student ID. 59300800007) and King Mongkut's University of Technology Thonburi (KMUTT).

REFERENCES

(1) Dahmen, N.; Lewandowski, I.; Zibek, S.; Weidtmann, A. Integrated lignocellulosic value chains in a growing bioeconomy: Status quo and perspectives. *GCB Bioenergy* **2019**, *11*, 107−117.
(2) Baruah, J.; Nath, B. K.; Sharma, R.; Kumar, S.; Deka, R. C.; Baruah, D. C.; Kalita, E. Recent Trends in the Pretreatment of Lignocellulosic Biomass for Value-Added Products. *Front. Energy Res.* **2018**, *6*, 141.
(3) Seidl, P. R.; Goulart, A. K. Pretreatment processes for lignocellulosic biomass conversion to biofuels and bioproducts. *Curr. Opin. Green Sustain.* **2016**, *2*, 48−53.
(4) Chen, H.; Liu, J.; Chang, X.; Chen, D.; Xue, Y.; Liu, P.; Lin, H.; Han, S. A review on the pretreatment of lignocellulose for high-value chemicals. *Fuel Process. Technol.* **2017**, *160*, 196−206.
(5) Ferreira, J. A.; Taherzadeh, M. J. Improving the economy of lignocellulose-based biorefineries with organosolv pretreatment. *Bioresour. Technol.* **2020**, *299*, 122695.
(6) Zhang, K.; Pei, Z.; Wang, D. Organic solvent pretreatment of lignocellulosic biomass for biofuels and biochemicals: A review. *Bioresour. Technol.* **2016**, *199*, 21−33.
(7) Inkrod, C.; Raita, M.; Champreda, V.; Laosiripojana, N. Characteristics of Lignin Extracted from Different Lignocellulosic Materials via Organosolv Fractionation. *Bioenergy Res* **2018**, *11*, 277−290.
(8) Agbor, V. B.; Cicek, N.; Sparling, R.; Berlin, A.; Levin, D. B. Biomass pretreatment: Fundamentals toward application. *Biotechnol. Adv.* **2011**, *29*, 675−685.
(9) Wang, S.; Bai, J.; Innocent, M. T.; Wang, Q.; Xiang, H.; Tang, J.; Zhu, M. Lignin-based carbon fibers: Formation, modification and potential applications. *Green Energy Environ.* **2021**, DOI: 10.1016/j.gee.2021.04.006.
(10) Borand, M. N.; Karaosmanoğlu, F. Effects of organosolv pretreatment conditions for lignocellulosic biomass in biorefinery applications: a review. *J. Renew. Sustain. Energy.* **2018**, *10*, 033104.
(11) Ho, M. C.; Ong, V. Z.; Wu, T. Y. Potential use of alkaline hydrogen peroxide in lignocellulosic biomass pretreatment and valorization—A review. *Renewable Sustainable Energy Rev.* **2019**, *112*, 75−86.
(12) Kabir, S. M. F.; Sikdar, P. P.; Haque, B.; Bhuiyan, M. A. R.; Ali, A.; Islam, M. N. Cellulose-based hydrogel materials: chemistry, properties and their prospective applications. *Prog. Biomater.* **2018**, *7*, 153−174.
(13) Shen, X.; Shamshina, J. L.; Berton, P.; Gurau, G.; Rogers, R. D. Hydrogels based on cellulose and chitin: fabrication, properties, and applications. *Green Chem.* **2016**, *18*, 53−75.
(14) Del Valle, L. J.; Díaz, A.; Puiggalí, J. Hydrogels for Biomedical Applications: Cellulose, Chitosan, and Protein/Peptide Derivatives. *Gels* **2017**, *3*, 27.
(15) Liu, Z.; Wang, H.; Liu, C.; Jiang, Y.; Yu, G.; Mu, X.; Wang, X. Magnetic cellulose-chitosan hydrogels prepared from ionic liquids as reusable adsorbent for removal of heavy metal ions. *Chem. Commun.* **2012**, *48*, 7350−7352.
(16) Zhao, X.; Cheng, K.; Liu, D. Organosolv pretreatment of lignocellulosic biomass for enzymatic hydrolysis. *Appl. Microbiol. Biotechnol.* **2009**, *82*, 815−827.
(17) Jang, S.-K.; Kim, H.-Y.; Jeong, H.-S.; Kim, J.-Y.; Yeo, H.; Choi, I.-G. Effect of ethanol organosolv pretreatment factors on enzymatic digestibility and ethanol organosolv lignin structure from Liriodendron tulipifera in specific combined severity factors. *Renew. Energy.* **2016**, *87*, 599−606.
(18) Mesa, L.; González, E.; Cara, C.; González, M.; Castro, E.; Mussatto, S. I. The effect of organosolv pretreatment variables on enzymatic hydrolysis of sugarcane bagasse. *Chem. Eng. J.* **2011**, *168*, 1157−1162.
(19) Zhang, X.; Yuan, Z.; Wang, T.; Zhang, Q.; Ma, L. Effect of the temperature on the dissolution of corn straw in ethanol solution. *RSC Adv.* **2016**, *6*, 102306−102314.
(20) Dutra, E. D.; Santos, F. A.; Alencar, B. R. A.; Reis, A. L. S.; de Souza, R. d. F. R.; da Silva Aquino, K. A.; Morais, M. A., Jr.; Menezes, R. S. C. Alkaline hydrogen peroxide pretreatment of lignocellulosic biomass: status and perspectives. *Biomass Convers. Biorefin.* **2018**, *8*, 225−234.
(21) Cabrera, E.; Muñoz, M. J.; Martín, R.; Caro, I.; Curbelo, C.; Díaz, A. B. Alkaline and alkaline peroxide pretreatments at mild temperature to enhance enzymatic hydrolysis of rice hulls and straw. *Bioresour. Technol.* **2014**, *167*, 1−7.
(22) Wu, Y.; Wu, J.; Yang, F.; Tang, C.; Huang, Q. Effect of H2O2 Bleaching Treatment on the Properties of Finished Transparent Wood. *Polymers* **2019**, *11*, 776.
(23) He, W.; Gao, W.; Fatehi, P. Oxidation of kraft lignin with hydrogen peroxide and its application as a dispersant for kaolin suspensions. *ACS Sustainable Chem. Eng.* **2017**, *5*, 10597−10605.
(24) Qu, L.-J.; Zhu, S.-F.; Liu, M.-J.; Wang, S.-Y. The mechanism and technology parameters optimization of alkali-H_2O_2 one-bath cooking and bleaching of hemp. *J. Appl. Polym. Sci.* **2005**, *97*, 2279−2285.
(25) Then, Y. Y.; Ibrahim, N. A.; Zainuddin, N.; Chieng, B. W.; Ariffin, H.; Yunus, W. M. Z. W. Influence of alkaline-peroxide treatment of fiber on the mechanical properties of oil palm mesocarp fiber/poly (butylene succinate) biocomposite. *BioResources* **2015**, *10*, 1730−1746.
(26) Zhang, H.; Huang, S.; Wei, W.; Zhang, J.; Xie, J. Investigation of alkaline hydrogen peroxide pretreatment and Tween 80 to enhance enzymatic hydrolysis of sugarcane bagasse. *Biotechnol. Biofuels.* **2019**, *12*, 107.
(27) Selig, M. J.; Vinzant, T. B.; Himmel, M. E.; Decker, S. R. The Effect of Lignin Removal by Alkaline Peroxide Pretreatment on the Susceptibility of Corn Stover to Purified Cellulolytic and Xylanolytic Enzymes. *Appl. Biochem. Biotechnol.* **2009**, *155*, 94−103.
(28) Damaurai, J.; Preechakun, T.; Raita, M.; Champreda, V.; Laosiripojana, N. Investigation of Alkaline Hydrogen Peroxide in Aqueous Organic Solvent to Enhance Enzymatic Hydrolysis of Rice Straw. *Bioenergy Res* **2021**, *14*, 122−134.
(29) Cabañas-Romero, L. V.; Valls, C.; Valenzuela, S. V.; Roncero, M. B.; Pastor, F. I. J.; Diaz, P.; Martínez, J. Bacterial cellulose−chitosan paper with antimicrobial and antioxidant activities. *Biomacromolecules* **2020**, *21*, 1568−1577.
(30) Fideles, T. B.; Santos, J. L.; Tomás, H.; Furtado, G. T. F. S.; Lima, D. B.; Borges, S. M. P.; Fook, M. V. L. Characterization of Chitosan Membranes Crosslinked by Sulfuric Acid. *OALib* **2018**, *05*, No. e4336.
(31) Adel, A.; El-Gendy, A.; Diab, M.; Abouzeid, R.; El-Zawawy, W.; Dufresne, A. Microfibrillated cellulose from agricultural residues. Part I: Papermaking application. *Ind Crops Prod* **2016**, *93*, 161−174.
(32) Sim, K.; Youn, H. J. Preparation of porous sheets with high mechanical strength by the addition of cellulose nanofibrils. *Cellulose* **2016**, *23*, 1383−1392.
(33) Phruksaphithak, N.; Sukthong, A.; Muanpannarai, W.; Theptong, A. Effect of Ammonium Sulfate on the Porous Creating of Regenerated Cellulose Hydrogel from Palm Oil Trunk. *Sci. Technol. Asia.* **2019**, *24*, 6−14.
(34) Al-Shamary, E. E.; Al-Darwash, A. K. Influence of fermentation condition and alkali treatment on the porosity and thickness of bacterial cellulose membranes. *Online J. Sci. Technol.* **2013**, *3*, 194−203.
(35) Delkumburewatte, G. B. Weft-knitted structures for moisture management. In *Advances in Knitting Technology*; Au, K. F., Ed.; Woodhead Publishing, 2011; pp 287−308.
(36) Hubbe, M. A.; Ayoub, A.; Daystar, J. S.; Venditti, R. A.; Pawlak, J. J. Enhanced absorbent products incorporating cellulose and its derivatives: A review. *BioResources* **2013**, *8*, 6556−6629.

(37) Correlo, V. M.; Pinho, E. D.; Pashkuleva, I.; Bhattacharya, M.; Neves, N. M.; Reis, R. L. Water Absorption and Degradation Characteristics of Chitosan-Based Polyesters and Hydroxyapatite Composites. *Macromol. Biosci.* **2007**, *7*, 354−363.
(38) Zhai, T.; Zheng, Q.; Cai, Z.; Xia, H.; Gong, S. Synthesis of polyvinyl alcohol/cellulose nanofibril hybrid aerogel microspheres and their use as oil/solvent superabsorbents. *Carbohydr. Polym.* **2016**, *148*, 300−308.
(39) Doshi, B.; Sillanpää, M.; Kalliola, S. A review of bio-based materials for oil spill treatment. *Water Res.* **2018**, *135*, 262−277.
(40) Laitinen, O.; Suopajärvi, T.; Österberg, M.; Liimatainen, H. Hydrophobic, superabsorbing aerogels from choline chloride-based deep eutectic solvent pretreated and silylated cellulose nanofibrils for selective oil removal. *ACS Appl. Mater. Interfaces* **2017**, *9*, 25029−25037.
(41) Kwon, G.-J.; Han, S.-Y.; Park, C.-W.; Park, J.-S.; Lee, E.-A.; Kim, N.-H.; Alle, M.; Bandi, R.; Lee, S.-H. Adsorption Characteristics of Ag Nanoparticles on Cellulose Nanofibrils with Different Chemical Compositions. *Polymers* **2020**, *12*, 164.
(42) Wahid, F.; Hu, X.-H.; Chu, L.-Q.; Jia, S.-R.; Xie, Y.-Y.; Zhong, C. Development of bacterial cellulose/chitosan based semi-interpenetrating hydrogels with improved mechanical and antibacterial properties. *Int. J. Biol. Macromol.* **2019**, *122*, 380−387.
(43) Ritonga, H.; Nurfadillah, A.; Rembon, F. S.; Ramadhan, L. O. A. N.; Nurdin, M. Preparation of Chitosan-EDTA hydrogel as soil conditioner for soybean plant (Glycine max). *Groundwater Sustainable Dev.* **2019**, *9*, 100277.
(44) Halász, K.; Csóka, L. Black chokeberry (Aronia melanocarpa) pomace extract immobilized in chitosan for colorimetric pH indicator film application. *Food Packag. Shelf Life.* **2018**, *16*, 185−193.
(45) Ngwabebhoh, F. A.; Gazi, M.; Oladipo, A. A. Adsorptive removal of multi-azo dye from aqueous phase using a semi-IPN superabsorbent chitosan-starch hydrogel. *Chem. Eng. Res. Des.* **2016**, *112*, 274−288.
(46) Zhao, G.; Lyu, X.; Lee, J.; Cui, X.; Chen, W.-N. Biodegradable and transparent cellulose film prepared eco-friendly from durian rind for packaging application. *Food Packag. Shelf Life.* **2019**, *21*, 100345.
(47) Alam, M. N.; Islam, M. S.; Christopher, L. P. Sustainable Production of Cellulose-Based Hydrogels with Superb Absorbing Potential in Physiological Saline. *ACS Omega* **2019**, *4*, 9419−9426.
(48) Lee, C. M.; Mittal, A.; Barnette, A. L.; Kafle, K.; Park, Y. B.; Shin, H.; Johnson, D. K.; Park, S.; Kim, S. H. Cellulose polymorphism study with sum-frequency-generation (SFG) vibration spectroscopy: identification of exocyclic CH2OH conformation and chain orientation. *Cellulose* **2013**, *20*, 991−1000.
(49) Cervera, M. F.; Heinämäki, J.; Krogars, K.; Jörgensen, A. C.; Karjalainen, M.; Colarte, A. I.; Yliruusi, J. Solid-state and mechanical properties of aqueous chitosan-amylose starch films plasticized with polyols. *AAPS PharmSciTech* **2004**, *5*, 109.
(50) Barros, S. C.; da Silva, A. A.; Costa, D. B.; Costa, C. M.; Lanceros-Méndez, S.; Maciavello, M. N. T.; Ribelles, J. L. G.; Sentanin, F.; Pawlicka, A.; Silva, M. M. Thermal−mechanical behaviour of chitosan−cellulose derivative thermoreversible hydrogel films. *Cellulose* **2015**, *22*, 1911−1929.
(51) Celebi, H.; Kurt, A. Effects of processing on the properties of chitosan/cellulose nanocrystal films. *Carbohydr. Polym.* **2015**, *133*, 284−293.
(52) Szymańska, E.; Winnicka, K. Stability of chitosan-a challenge for pharmaceutical and biomedical applications. *Mar. Drugs* **2015**, *13*, 1819−1846.
(53) Król-Morkisz, K.; Pielichowska, K. Thermal Decomposition of Polymer Nanocomposites With Functionalized Nanoparticles. In *Polymer Composites with Functionalized Nanoparticles*; Pielichowski, K., Majka, T. M., Eds.; Elsevier, 2019, pp 405−435.
(54) Sluiter, A.; Hames, B.; Ruiz, R.; Scarlata, C.; Sluiter, J.; Templeton, D.; Crocker, D. *Determination of Structural Carbohydrates and Lignin in Biomass Laboratory Analytical Procedure*; National Renewable Energy Laboratory, 2012.
(55) Mussatto, S. I.; Rocha, G. J. M.; Roberto, I. C. Hydrogen peroxide bleaching of cellulose pulps obtained from brewer's spent grain. *Cellulose* **2008**, *15*, 641−649.
(56) Fischer, E. R.; Hansen, B. T.; Nair, V.; Hoyt, F. H.; Dorward, D. W. Scanning electron microscopy. *Current Protocols in Molecular Biology*; John Wiley & Sons 2012; Chapter 2, Unit2B.2-2B.2.
(57) Tanpichai, S.; Witayakran, S.; Srimarut, Y.; Woraprayote, W.; Malila, Y. Porosity, density and mechanical properties of the paper of steam exploded bamboo microfibers controlled by nanofibrillated cellulose. *J. Mater. Res. Technol.* **2019**, *8*, 3612−3622.
(58) Mohamed, S. A.; El-Sakhawy, M.; Kamel, S. Water Resistance and Antimicrobial Improvement of Bagasse Paper by Microwave Modification with Fatty Acid and Ag-NPS Nanocomposite. *Cellul. Chem. Technol.* **2017**, *52*, 423−431.
(59) Sun, F. F.; Wang, L.; Hong, J.; Ren, J.; Du, F.; Hu, J.; Zhang, Z.; Zhou, B. The impact of glycerol organosolv pretreatment on the chemistry and enzymatic hydrolyzability of wheat straw. *Bioresour. Technol.* **2015**, *187*, 354−361.
(60) Ioelovich, M. Crystallinity and hydrophility of chitin and chitosan. *Res. Rev.: J. Chem.* **2014**, *3*, 7−14.

https://doi.org/10.1021/acsomega.1c03141
ACS Omega 2021, 6, 22791−22802